A microfluidic distributor combining minimal volume, minimal dispersion and minimal sensitivity to clogging

Jespers, Sander; Deridder, Sander; Desmet, Gert

Published in:
Journal of Chromatography A

DOI:
10.1016/j.chroma.2018.01.029

Publication date:
2018

A Microfluidic Distributor Combining Minimal Volume, Minimal Dispersion and Minimal Sensitivity to Clogging

Sander Jespers, Sander Deridder, Gert Desmet*
Vrije Universiteit Brussel, Department of Chemical Engineering, Pleinlaan 2, 1050 Brussels, Belgium
Corresponding author (tel: +32 2629 32 51, e-mail: gedesmet@vub.ac.be)

Abstract

A new type of microfluidic flow distributor (referred to as the mixed mode or MM-distributor) is proposed. Its performance characteristics are determined using computational fluid dynamics (CFD), both in the absence and the presence of clogging, which is an important problem in microfluidic systems. A comparison is made with two existing, well-performing distributor types: the bifurcating (BF) distributor and an optimized diverging distributor, the so-called radially interconnected (RI) distributor.

It was found that, in the absence of clogging, the MM-distributor produces only a little more dispersion than the bifurcating (BF) distributor, but much less than the radially interconnected (RI) distributor. The dispersion in an MM-distributor also follows a similar dependency on its width (power≅2) as the BF-distributor. The dispersion in the RI-distributor on the other hand displays a very disadvantageous 4^{th}-order dependency on its width, prohibiting its use to distribute the flow across wide beds (order of millimeters or centimeters). These observations hold independently of the flow rate.

With increasing degree of clogging, the MM-distributor rapidly becomes advantageous over the BF-distributor, owing to the fluid contact zones that are provided after each bifurcation step. This means that overall, and when the occurrence of clogging cannot be excluded, the MM-type distributor seems to offer the best possible compromise between the ability to cope with local clogging events and the dispersion in the absence of clogging.

Keywords

Flow distribution, microfluidic devices, computational fluid dynamics, dispersion, residence time distribution

1. Introduction

The design of novel microfluidic flow distributors to make the transition from a narrow connection channel or tube to a wide separation or reaction channel and vice versa with a minimum of dispersion remains a topic of interest [1-12]. The development of well-performing fluid distributors is especially important in applications where a uniform residence time is important or where axial dispersion has to be minimized, such as in plug flow reactors, membrane separations, and chromatography-on-chip [13-15]. Recently, computational fluid dynamics has gained interest as a tool for the design and optimization of microfluidic structures, as it circumvents experimental complications and allows unambiguous interpretation of the results [16-19].

Maybe the most iconic microfluidic distributor is that proposed in the seminal paper by the Regnier group on microfabricated CEC and LC columns [20]. In the present study, this distributor will be referred to as the bifurcating (BF) distributor, as it is characterized by the fact that it consecutively splits each channel in 2 sub-channels, leading to 2^n distribution channels of equal length, where n is the number of consecutive splits. Whereas the distributor used by the Regnier group was designed such that the velocity remained the same at every bifurcation level (necessitating the use of fairly broad distributor channels in the first few splitting stages), numerically studies in our group showed that much less dispersion is obtained if the distributor channels remain equally wide at all bifurcation levels [2]. In the present study, we therefore always considered the latter design for the BF-distributor (see Fig. 1a).

Another class of distributors merely spreads the flow via a diverging section. This can be either empty, or filled with microstructures (pillars). As demonstrated convincingly by Sant *et al.*[7], the presence of the pillars can reduce the dispersion losses with at least 50% compared to the case of an open diverging section. As shown by Vangelooven *et al.* [5] another major improvement can be obtained if the pillars are stretched out in the radial direction, to promote radial dispersion (see Fig. 1b). This type of distributor will be further referred to as the radially-interconnected (RI) distributor type, to distinguish it from the BF-type distributors, where the flow paths in the distributor never make contact again once they bifurcated.

Considering a BF-distributor of the type shown in Fig. 1a, i.e., with a constant channel width, the BF-distributor is irrevocably the distributor type requiring the smallest volume to perform the distribution task. Given that dispersion is generally strongly dominated by the volume of the system, this gives the BF-distributor an important advantage [2]. Another clear advantage of the BF-distributor is that all flow paths have the same trajectory length, whereas the RI-distributor obviously has different flow path lengths (shorter through the center than through the sides).

An important drawback of the BF-type distributor, however, is that it is very sensitive to local clogging. If one of the channel segments in the distributor gets clogged, all subsequent channels branching away from it will be affected, as they only receive liquid from the clogged “mother” segment. This is where the RI-type distributors can prove advantageous, because they can use their radial mixing and the fact that there is full contact between the different liquid streams at all levels to overcome such local clogging. However, little is known about how important this advantage is. One reason for this lack of information is that it is difficult to investigate this experimentally, as the reproducibility and quantification of the clogging one can induce in real life is difficult. A recent study by Davydova *et al.* [1] looking at the clogging characteristics of different flow distributors therefore used computational fluid dynamics (CFD). They concluded that BF-distributors, due to their minimal volume, perform better than RI-distributors if no clogging is present, whereas it is only when substantial clogging (more than 50%) occurs in a channel that the RI-distributor can be expected to outperform the BF-distributor. Their study was however conducted by considering systems with very wide channels, where the dispersion could be dominated by dispersion in the individual segments.

What we propose here is a new type of distributor (referred to hereafter as the mixed mode, or MM, distributor) that combines the positive aspects of both the BF-and RI-distributor types. In a MM-type of distributor, every flow path still goes through a succession of bifurcations, but a contact zone is provided after each splitting stage wherein all different flow paths are again in direct fluidic contact. Preferentially, this contact zone is either very short, or filled with pillars or any other kind of flow distributor elements. To ensure that every flow path running from the single inlet to the final row of distributor outlets has the same length, these pillars should be aligned in an even number of rows (n=0,2,4,..) and the radial positions of the centerlines of the different inter-pillar spaces at every n^{th} row in the contact zone should match these of the outlets of the preceding bifurcation step, while the radial positions of the centerlines of the different inter-pillar spaces at every $n\text{-}1^{th}$ row should match the centerlines of the pillars in the following row.

It can be inferred that the presence of the contact zones might alleviate the clogging sensitivity of the conventional BF-distributor, whereas the main advantage of the latter, i.e., that all flow paths have the same length, remains preserved provided the above design rules are obeyed. Fig. 1c and 1d show two possible designs according to this concept. In one design (MM_I, Fig. 1c), each fluidic contact zone consists of two rows of flat-rectangular pillars to promote radial dispersion. In the second design (MM_{II}, Fig. 1d), the flat-rectangular pillars are missing and the contact zone only consists of a single open-channel space. It goes without saying that more complex designs of the MM-flow distributor type can easily be conceived wherein the number of flat-rectangular pillar rows is not the same at every bifurcation level, e.g., to leave more possibility for fluid remixing at the earlier stages of bifurcation than at the later stages.

In the present study, we have quantitatively assessed the potential advantage of MM-distributors by comparing its dispersion characteristics to the best possible representatives of the BF and RI-type distributors. To avoid experimental complications, this was done numerically, using computational fluid dynamics (CFD). Except for the part in Section 3.3, all distributors always had the same inlet and the same number of outlet ports, and had to handle the same flow rate. To allow investigating a high number of conditions and geometries in a reasonable time, all simulations were done in 2D, neglecting the additional dispersion one can expect from the top and bottom wall that are present in practice [21]. Including this effect would have added an extra variable and would have consumed roughly a 10- to 100-fold of computational time (depending on the selected aspect ratio of the channels). It has furthermore been demonstrated in literature that the additional dispersion originating from the 3D-geometry can be considered as an independent extra term, especially when the channels have a high aspect-ratio, i.e. when the channels are significantly deeper than wider, which is anyhow the condition resulting from a design aiming at a minimal distributor volume (keeping the depth of the channels constant) [22]. Furthermore, since the extra dispersion from the top and bottom wall contribution can be expected to be proportional to the time spend in the distributor, and since this grows from BF over MM to the RI-distributor, it can be inferred the addition of this effect will only enhance the presently observed differences.

2. Considered Geometries and Simulation Conditions

2.1 Geometries and flow and fluid parameter

Fig. 1a-d shows the different considered distributor geometries, i.e. the BF-, MM_I-, MM_{II}-, and RI-distributors, respectively. The red line in each of the distributors depicts the species monitor line, used to detect the species plug exiting the distributors. Each distributor was also provided with a porous zone at the 4-outlet-level, in the outer most channel (see red boxes in Figs 1a-d). This zone had a tunable permeability, allowing to easily change the local flow resistance to simulate different degrees of clogging in the distributor without having to make different drawings. To reduce the simulation time, only one half of each geometry is simulated since the distributors are anyhow symmetrical (see e.g., Fig. 2 further on).

Fig. 1e shows a zoomed view of the inlet of each of the distributors, as well as an example of the employed computational grid (mesh) size and shape. The red dashed box in Fig. 1e delimits the cells which are part of the “injection box” (100 cells in total). The cells in this injection box are patched with 1 % species as the starting condition for the simulation. The flat-rectangular distributor elements (used here as an alternative to the radially-elongated diamonds used in [1,2,4,5]) at the outlet of each distributor (and for the RI-distributor over the entire geometry) were 30 µm wide and 2.5 µm thick. For the BF-and MM-distributors, the length of the flat-rectangular distributor elements used in a previous splitting step (when following the direction of fluid flow) was taken equal to twice the length of the elements used after the splitting step plus the width of one distributor flow-through channel. These channels were 2.5 µm wide throughout the entire geometry for every distributor. The distributors all fed into a 5 cm long bed filled with the same flat-rectangular elements as used at the outlet of the distributor (see the row of pillars after the red line in Figs. 1a-d).

The fluid used in the simulations was liquid water with a viscosity of 1.003 cP and a density of 998.2 kg/m³. The flow rate was chosen so that a linear velocity of approximately 0.25 mm/s was achieved in the reaction channel following the distributor (a practically relevant linear velocity for microchip chromatography). The species that was traced during the simulations was water as well. This mixture of water in water was given a self-diffusivity of 10^{-9} m²/s.

2.2 Numerical Methods

All simulations were performed with Ansys® Workbench version 16.2 from Ansys, Inc., purchased from Ansys Benelux, Wavre, Belgium. Within this software platform all flow domains were drawn with Ansys® Design Modeler and meshed with Ansys® Meshing. All simulations were performed with Ansys® Fluent.

Mesh

The mesh size was chosen such that the shortest flow domain contained 10 mesh cells. The mesh consisted of quadrilateral cells. To check mesh independency, a mesh containing cells half the original size, resulting in a quadruple cell count, was used. For the 500 µm wide BF-distributor, the difference in plate height recorded with this finer mesh was only 3.5% smaller than for the original mesh. It was therefore concluded the original mesh yields sufficient accuracy, at least for this comparative study.

Solver

First, the velocity fields were computed solving the Navier-Stokes equations using the segregated pressure-based steady-state solver. For the spatial discretization, the least squares cell based method was used to calculate concentration gradients, the coupled scheme for pressure-velocity coupling, the second order interpolation scheme for pressure and second order upwind scheme for momentum. Boundary conditions were set to wall for the side walls and sides of the flat-rectangular pillars, the inlet plane was put at a fixed mass-flow rate and the outlet plane were set to outflow. The porous zone was set to interior.

Subsequently, the 100 mesh cells of the injection box were patched with 1% species. The transient solver, with first order implicit temporal discretization and second order upwind scheme for spatial discretization, was then used to solve the convection diffusion equation yielding the transient concentration field of species band migrating through the flow domain. A fixed time stepping method with 10000 steps of size 1.10^{-6} s was used.

Hardware

All simulations were performed on Dell Power Edge R210 Rack Servers each equipped with an Intel Xeon x3460 processor (clock speed 2,8 GHz, 4 cores) and 16 Gb, 1333 MHz ram memory, running on Windows server edition 2008 R2 (64-bit). Simulations of the steady-state velocity field in the aforementioned geometries took about 1 hour, while the transient species concentration field simulations took about 24 hours.

2.3 Data processing method

For each simulation, the mass fraction of species passing the "monitor" line (see red lines in Figs. 1a-d) was recorded as a function of time. From the resulting peaks, the time-based variance (σ_t^2) and mean elution time ($\bar{t}$) were calculated using the mathematical moments of the peaks.

$$\bar{t} = \int t \cdot c(t) dt$$

$$\sigma_t^2 = \int (t - \bar{t})^2 \cdot c(t) dt = \int t^2 \cdot c(t) dt - \bar{t}^2$$

wherein c(t) is the mass fraction of species as a function of time. From these values, the volumetric variance (σ_v^2) can be calculated with

$$\sigma_v^2 = \sigma_t^2 \cdot F^2$$

Using σ_v^2 (which contains information of F) instead of σ_t^2 as a measure of the peak width eliminates the influence the flow rate has on the observed (time-based) peak width.

3. Results and Discussion

3.1 Initial comparison (base case)

In a first set of simulations, the goal was to determine which of the four considered distributor types has the best performance in the absence of clogging. Fig. 2 shows a framed image of the species band at the moment of elution for each of the 4 considered distributor types. Fig. 3 shows the corresponding time responses (peaks) as recorded on the monitor line.

Table 1 shows the numerical values for $\bar{t}$ and σ_v^2 of each of the peaks, as well as the pressure drop between the inlet and the monitor line. As expected from its low volume and the uniform length of its flow-through channels, the BF-distributor leads to the narrowest peak (σ_v^2= 0.013 nL²) and elutes the fastest. The peak leaving the RI-distributor, on the other hand, is the widest, with the longest mean elution time and exhibits strong peak tailing. This obviously corresponds to its larger volume, and is also reflected by the fact that the σ_v^2-value of the RI peak (σ_v^2=0.165 nL²) is more than 10-fold higher than that of the BF peak (σ_v^2=0.013 nL²). The two MM-distributors lead to peaks with intermediate mean elution times and widths, but without the tailing of the RI-distributor. In line with the difference in volume, the MM_I-distributor has a larger residence time and produces more dispersion than the MM_{II}-distributor (σ_v^2= 0.026 nL² for MM_I while σ_v^2= 0.017 nL² for MM_{II}). Another important observation from Fig. 2 is that the BF-, as well as the MM-type distributors produce species bands that are perfectly uniform in the radial direction (reflecting the fact that all possible flow-through paths have the same length), whereas the RI-distributor clearly produces a warped band. The latter obviously is caused by the difference in flow-path length between the central and the outer region. Apparently, this difference cannot be overcome by the strong radial mixing induced by the radially elongated elements in the RI-distributor.

Also shown in Table 1 are the pressure drops over the distributors. Here, the RI distributor is more advantageous, because the flow is very rapidly divided over many flow paths so that the local velocity (which obviously is highest at the inlet) drops rapidly. This is not the case in the BF-distributor, where the highest flow rates (F/2 after first bifurcation, F/4 after 2nd bifurcation,…) are maintained over the longest distance (=length of flow-through channels). As a consequence, the BF-distributor requires a larger pressure-drop. The two MM-type distributors have even a larger pressure drop, because of the presence of the contact zones which increases the fluid path length and hence generates an extra pressure drop.

Table 1. Comparison of mean elution, volumetric variance, and pressure drop for the different distributor types in the absence of clogging at a flow rate of 1.32 µL/min.

	RI	**MM_I**	**MM_{II}**	**BF**
$\bar{t}$ (s)	0.100	0.100	0.057	0.032
σ_v^2 (nL²)	0.165	0.026	0.017	0.013
Δp (bar)	3.5	11.2	8.7	7.7

If the extra pressure-drop of the MM-distributor would be an issue, designs can be conceived wherein the flow-through channels are widest near the inlet of the distributor and become narrower towards its exit. The optimal variation of the channel width will depend on the compromise between the extra dispersion and the pressure drop.

The next set of simulations mainly aimed at determining which of the two new distributors (MM_I or MM_{II}) performs best in the presence of clogging. For these measurements, the porous zone in the red boxes shown in Figs. 1a-d was tuned to reflect a 70% clogging (=70% of the channel cross section area is supposed to be blocked over a length of 2.5 µm) of the outer most channel at the 4-outlet-level (see position of red boxes in Fig 4.).

Fig. 4 and 5 respectively show the bands at the moment of elution from the distributors and the corresponding peaks. Table 2 shows the numerical values for $\bar{t}$ and σ_v^2 of each peak. As can be noted, the peak from the BF-distributor becomes considerably wider (σ_v^2= 0.45 nL²) and shows an extreme tailing and asymmetry compared to the non-clogged case in Figs. 2a-3a. The reason for this is that the BF-distributor has no flow paths going around the clogging and can hence not correct for errors. Part of the injected species even clearly get stuck in the region near the congestion (see added dashed oval). This also explains why the mean elution time becomes longer than in the non-clogged case.

Table 2. Comparison of the mean elution time and the volumetric variance for the different distributor types with 70 % clogging of the outer most channel at the 4-outlet-level and a flow rate of 1.32 µL/min.

	RI	**MM_I**	**MM_{II}**	**BF**
$\bar{t}$ (s)	0.100	0.100	0.061	0.040
σ_v^2 (nL²)	0.271	0.223	0.532	0.450

On the other hand, the clogging has hardly any effect on the peak shape in case of the RI-distributor. The peak width (σ_v^2= 0.271 nL²), mean elution time, and symmetry are all almost identical to the results obtained without clogging. This confirms the excellent ability of RI-type distributors to cope with local clogging events, which is due to its strong radial mixing and the many different flow paths the fluid can take to circumvent the clogged area.

Again, the MM-distributors show an intermediate behavior. However, whereas the MM_{II}-distributor performs close to the unfavorable behavior of the BF-distributor (the σ_v^2 increased to 0.532 nL^2), the MM_I-distributor performs better (σ_v^2= 0.223 nL^2). Here again, the explanation can be found in the geometry of the distributors. The contact zones in the MM_{II}-distributor are minimally small and and are reduced to a single flow-through channel. This gives the fluid only a limited possibility to compensate for errors. In the MM_I-distributor, three of such channel layers are present in each contact zone, giving the fluid much more time to redistribute across the entire width of the distributor. To understand this further, it is instructive to compare the bands leaving the MM_I-and MM_{II}-distributors in Fig. 4. Whereas the band leaving the distributor in the MM_I-distributor substantially fills the entire width of the channel (reflecting the ability of this distributor to overcome the obstruction blocking a branch feeding the most rightward part of the distributor), the band in the MM_{II}-distributor clearly hasn't yet been able yet to reach the most rightward part of the distributor when leaving the distributor.

Since the MM_{II}-distributor is outperformed by the BF-distributor under ideal circumstances (no clogging) and by the MM_I-distributor when clogging is possible, it was decided to omit this design from all further calculations.

3.2 Effect of F

For the three distributors that remained under consideration (BF, RI, and MM_I), the effect of the flow rate on the volumetric variance σ_v^2 of the bands leaving the distributor was examined. These simulations were conducted in the absence of clogging, to obtain the most simple and direct insight. Five different flow rates were applied to each of the distributors: 1.32 µL/min (corresponding to the optimal linear velocity of 0.25 mm/s for chromatography in the reaction channel following the distributor), 1.98 µL/min, 2.64 µL/min, 3.96 µL/min, and 5.28 µL/min. The results of these calculations are shown in Fig. 6, and confirm the observations from Figs. 2-3 and Table 1 (MM in between BF and RI, but much closer to the BF than to the RI).

It is also striking to observe that the σ_v^2-values are nearly independent of the applied flow rate for all three distributors. Trying to explain this, we considered the analytical expression for the dispersion in a single microfluidic channel. Admittedly, the latter may only be a very crude representation of the flow-through channels in the distributors, but the availability of an analytical expression at least allows to understand some of the dispersion dynamics. As can be derived from Broeckhoven and

Desmet [23] and Vanderlinden *et al.*[24] the volumetric variance of a band travelling through a straight tube under fully-developed and dispersion dominated laminar flow conditions is given by:

$$\sigma_V^2 = \alpha \cdot \frac{d_{tube}^4 \cdot F \cdot L}{D_m} \cdot \left[1 - \frac{1}{\beta L}(1 - e^{-\beta L}) \right] \tag{1}$$

Where α is a constant depending on the geometry of the tube (α =1/105 for a channel formed between two parallel plates) and $\beta = 15\pi D_m/F$.

Using Eq. (1) to calculate σ_v^2 as a function of F, with d_{tube}=2.5 µm, D_m=1.10^{-9} m²/s and L the length of the flow path from the inlet to any of the outlet points (RI= 26.5 µm, BF= 25.125 µm, MM_I= 56.125 µm) shows that the dispersion in the flow-through channels is not fully-developed yet (i.e., σ_v^2/L is not yet a constant). In other words, the flow rate is so high that the factor between straight brackets in Eq. (1) still varies in a nearly inversely proportional way with F, thus approximately compensating for the linear F-dependency preceding the straight brackets. This then explains the near-constant σ_v^2-values in Fig. 6. It is only when L would be significantly larger, or F would be significantly smaller that the factor between straight brackets would converge to unity. In this way, the linear F-dependency of the first factor remains the only flow rate effect, and a linear relation between σ_v^2 and F would be achieved.

Since the flow rate obviously doesn't have a significant influence on σ_v^2, all subsequent simulations were done at a flow rate of 1.32 µL/min, as this corresponds to a practically relevant linear velocity.

3.3 Effect of the distributor width

To assess how the final distributor width affects the conclusions from the previous sections (no clogging case), the σ_v^2 was measured for different channel widths, again in the absence of clogging. The change in channel width was achieved by adding or eliminating layers to the distributors and by increasing or decreasing the number of outlets, in other words, the dimensions of the flow-through channels and the flat-rectangular pillars in the bed and the last rows of pillars in the distributor were kept the same. Note that, whereas the RI-distributor can have any number of outlets, the MM_I-and BF-distributors can only have 2^n outlets, with n an integer. Moreover, when fewer than 8 outlets are considered, there is no difference between the MM_I-and BF-distributor. Hence, for the MM_I-and BF-distributor 3 cases were studied: 250 µm (8 outlets), 500 µm (16 outlets), and 1000 µm (32 outlets) wide final channels, while for the RI-distributor, the same 3 cases were studied, as well as an additional two cases of 375 µm(12 outlets) and 750 µm (24 outlets). The flow rate was scaled in proportion with the final distributor width, as each distributor is assumed to feed into a reaction or separation bed with a width equal to that of the distributor and we wanted to keep the linear velocity in this bed the same for all considered channel widths. The results of these simulations are shown in Fig. 7 (data points) as well as the corresponding fitted power law-curves.

As expected, given the absence of clogging, the BF-distributor has the lowest σ_v^2 in each case, the RI-distributor has the highest, and the MM_I produces variances that are larger the BF-distributor, but much smaller than those produced by the RI-distributors. The latter becomes more and more outspoken at the largest distributor widths, because the σ_v^2-values produced by the RI-distributor shows a proportionally greater increase with the distributor width than the MM_I-and BF-distributors. This is quantified by the power equation that can be fitted through the data points of each distributor type. As can be noted from the power law fittings in Fig. 7, the RI-distributor grows with the distributor width with a significantly higher power (3.8) compared to the MM_I-and BF-distributors (2.3 and 2.1 respectively). Roughly, this behavior can be understood as follows. To increase in width, the RI-distributor not only increases in width but also increases in length (given its overall triangular shape). Its volume hence increases ~width^2. Considering furthermore that the variance of any flow system in a first approximation scales with the square of its volume, we understand the observed width^4-increase. For the MM_I-and BF-distributors the volume grows essentially in the width and not in the length, such that the volume essentially increases in a near-linear way with the width and such that σ_v^2~width^2 (given that to a first approximation always σ_v^2~volume^2). As can be noted from Fig. 7, this 2nd-order dependency is indeed close to the observed power law dependency.

The fact that the MM_I-and BF-distributors have a variance that increases with a power close to 2 (σ_v^2~width^2) is very beneficial, because the dispersion in the uniform bed zone proceeding the distributor, can, for a given flow rate, also be expected to vary according to width^2. This implies the relative contribution of the distributor to the overall dispersion will remain the same when trying to use ever wider channels. Obviously, this is a highly beneficial characteristic. The near-4th power dependency of the RI-distributor implies a totally different behavior, as the relative contribution of the distributor (increasing with width^4) to the total dispersion will eventually always overwhelm that of the bed (increasing with width^2) when trying to maximize the bed width.

3.4 Detailed study of the effect of different degrees of clogging

Finally, the sensitivity to clogging of the different distributor types (BF, RI, and MM_I) was studied in more detail by considering step changes in the percentage of clogging induced in the porous zone indicated in Figs. 1a-d (red box). The flow rate was kept constant at 1.32 µL/min in all simulations.

As can be seen in Fig. 8, the volumetric variance σ_v^2 (0.165 µL²) of the RI-distributor at 0% clogging is approximately 10 fold higher than that of the BF-or MM_l-distributor (σ_v^2=0.165 µL² versus σ_v^2=0.013 µL² to 0.026 µL²). However, when the degree of clogging increases, the σ_v^2-values of the RI-distributor rise only relatively slowly from 0.165 µL² to 0.295 µL². This is in sharp contrast with the BF-distributor which, as already stated in section 3.1, produces the lowest at 0% clogging (σ_v^2=0.013 µL²) but exhibits a very steep rise in σ_v^2 when increasing the amount of clogging, reaching a maximum of 1.16 µL² at 90% clogging. This confirms our physical expectations and the results obtained by Davydova *et al.*[1], i.e., that the RI-distributor can cope much better with clogging defects than a BF type distributor.

The variance produced by the MM_l-distributor at 0% clogging is almost double that of the BF-distributor at 0.026 µL² but this value rises much less steeply with the degree of clogging than the BF-distributor. As a consequence, the σ_v^2 of the MM_l-distributor drops below that of the BF-distributor at approximately 15% clogging. After this point, the MM_l-distributor stays the lowest of the three distributors until 75% clogging, where it briefly rises above the RI-distributor before falling back down to 0.031 µL² at 80% clogging.

The unexpected drop in the variance produced by the MM_l that occurs at 80% clogging can be explained as follows. Considering that only a small amount of species enters the clogged channel (see dashed oval in Fig. 4), it is important to realize this fraction leaves the clogged channel only very slowly, as the velocity in the clogged channel is much lower than the velocity in the other channels due to the clogging. As a consequence, it gets diluted below the detection limit (<0.1 % of the maximum of the peak) by the time it reaches the detector (or in our case the red monitor line). In other words, the second peak of the MM_l signal in Fig. 5 (indicated by the small arrow) drops below the detection limit when the clogging degree exceeds 75 %.

A similar effect (i.e., the species in the clogged channel leaving only very slowly) occurs in the BF-distributor, but is in this case overshadowed by the asymmetry of the band that leaves the BF-distributor (Fig.4). In fact, part of the species that flow through the unclogged channels leak into the channels downstream the clogging zone (red curved arrow Fig 4), as the total pressure is lower there, before flowing out the distributor completely leading to heavily tailed peaks (Fig. 5) and hence high σ_v^2-values.

Obviously, the pattern of overtaking curves observed in Fig. 8 may be different when the clogging occurs at a different place, or when there are multiple clogging spots, or when the distributor width is different. Nevertheless, the general conclusions can be expected to remain the same, i.e., the BF-distributor will be superior at zero or very low % of clogging, whereas the MM-concept becomes advantageous as soon as the clogging becomes significant, because of its contact zones that allow for a redistribution of the flow after each bifurcation. The number of flow distributor rows (n) in these contact zones should be selected based on the probability for clogging. When it is deemed this probability is larger near the inlet, it seems straightforward to provide contact zones with a higher n near the inlet and with a lower n near the outlet.

4. Conclusions

A new type of microfluidic flow distributor (referred to as the mixed mode or MM-distributor) is proposed. It consists of flow paths undergoing a succession of bifurcations, with contact zones arranged after each splitting stage wherein the different parallel flow paths come again in direct fluidic contact. The contact zones are filled with flat-rectangular flow distributor elements designed such that all parallel flow-through paths through the distributor have the same length. In this design, each contact zone may consists of an even number of flow distributor element rows (n=0,2,4,..). Computational fluid dynamics (CFD) simulations showed that, in the absence of clogging, the MM-distributor produces only a little more dispersion than the bifurcating (BF) distributor, but much less than the radially interconnected (RI) distributor. The dispersion in an MM-distributor also follows a similar width-dependency (power≅2) as the BF-distributor. The dispersion in the RI-distributor on the other hand displays a very disadvantageous 4^{th}-order dependency, prohibiting its use to distribute the flow across wide beds (order of millimeters or centimeters). These observations hold independently of the flow rate.

With increasing degree of clogging, the MM-distributor rapidly becomes advantageous over the BF-distributor, owing to the fluid contact zones that are provided after each bifurcation step. This means that overall, when the occurrence of clogging cannot be excluded, the MM-type distributor seems to offer the best possible compromise between the ability to cope with local clogging events and the dispersion in the absence of clogging.

Interestingly, it has also been observed that, for some extreme cases of local clogging, the dispersion can become so strong that the species engaged in the clogged part of the distributor are smeared out so strongly that they fall below the detection limit (set here at 0.1% of the peak maximum). In this case, a higher degree of clogging leads to a smaller observed dispersion.

5. Acknowledgement

S.J. gratefully acknowledges Research grant from the Research Foundation Flanders (FWO Vlaanderen).

References

[1] E. Davydova, S. Wouters, S. Deridder, G. Desmet, S. Eeltink and P.J. Schoenmakers, Design and evaluation of microfluidic devices for two-dimensional spatial separations, *J. Chromatogr. A*, 2016, **1434**, 127.

[2] E.Davydova, S. Deridder, S. Eeltink, G. Desmet and P.J. Schoenmakers, Optimization and evaluation of radially interconnected versus bifurcating flow distributors using computational fluid dynamics modelling, *J. Chromatogr. A*, 2015, **1380**, 88.

[3] H. Liu and P. Li, Even distribution/dividing of single-phase fluids by symmetric bifurcation of flow channels, *Int. J. Heat Fluid Flow*, 2013, **40**, 165.

[4] J. Vangelooven, S. Schlautman, F. Detobel, H. Gardeniers and G. Desmet, Experimental optimization of flow distributors for pressure-driven separations and reactions in flat-rectangular microchannels, *Anal. Chem.*, 2011, **83**, 467.

[5] J. Vangelooven and G. Desmet, Computer aided design optimisation of microfluidic flow distributors, *J. Chromatogr. A*, 2010, **1217**, 6724.

[6] J. Vangelooven, W. De Malsche, J. Op De Beeck, H. Eghbali, H. Gardeniers and G. Desmet, Design and evaluation of flow distributors for microfabricated pillar array columns, *Lab Chip*, 2010, **10**, 349.

[7] H. J. Sant, J.W. Kim and B.K. Gale, Reduction of end-effect induced zone broadening in field-flow fractionation channels, *Anal. Chem.*, 2006, **78**, 7978.

[8] L. Luo and D. Tondeur, Optimal distribution of viscous dissipation in a multi-scale branched fluid distributor, *Int. J. Therm. Sci.*, 2005, **44**, 1131.

[9] D. Tondeur and L. Luo, Design and scaling laws of ramified fluid distributors by the constructal approach, *Chem. Eng. Sci.*, 2004, **59**, 1799.

[10] E.V. Rebrov, J.C. Schouten and M.H.J.M. de Croon, Single-phase fluid distribution and heat transfer in microstructured reactors, *Chem. Eng. Sci.*, 2011, **66**, 1374.

[11] J.I. Molho, A.E. Herr, B.P. Mosier, J.G. Santiago and T.W. Kenny, Optimization of turn geometries for microchip electrophoresis, *Anal. Chem.*, 2001, **73**, 1350.

[12] J.C. Giddings, M. Schure, M. Myers and G. Velez, End effects in field-flow fractionation channels: theory and means for reducing incremental zone broadening, *Anal. Chem*., 1984, **56**, 2099.

[13] J.P. Kutter, S.C. Jacobson and J.M. Ramsey, Integrated microchip device with electrokinetically controlled solvent mixing for isocratic and gradient elution in micellar electrokinetic chromatography, *Anal. Chem.*, 1997, **69**, 5165.

[14] Y. Song, M. Noguchi, K. Katatsuki, T. Sekigushi, J. Mizuno, T. Funatsu, S. Shoji and M. Tsunoda, Integration of pillar array columns into a gradient elution system for pressure-driven liquid chromatography, *Anal. Chem.*, 2012, **84**, 4739.

[15] G. Ocvirk, E. Verpoorte, A. Manz and H.M. Widmer, Integration of a micro liquid chromatograph onto a silicon chip, presented in part at Transducers ’95 - Eurosensors IX, Stockholm, June, 1995.

[16] J. Aubin, L. Prat, C. Xuereb and C. Gourdon, Effect of microchannel aspect ratio on residence time distributions and the axial dispersion coefficient, *Chem. Eng. Process.*, 2009, **48**, 554.

[17] A.G. Kanaris and A.A. Mouza, Numerical investigation of the effect of geometrical parameters on the performance of a micro-reactor, *Chem. Eng. Sci.*, 2011,**66**, 5366.
[18] T. Glatzel, C. Litterst, C. Cupelli, T. Lindemann, C. Moosmann, R. Niekrawietz, W. Streule, R. Zengerle and P. Koltay, Computational fluid dynamics (CFD) software tools for microfluidic applications–A case study, *Comput. Fluids*, 2008, **37**, 218.
[19] S. Yang, A. Ündar and J.D. Zahn, A microfluidic device for continuous, real time blood plasma separation, *Lab Chip*, DOI: 10.1039/b516401j
[20] B. He and F. Regnier, Microfabricated liquid chromatography columns based on collocated monolith support structures, *J. Pharm. Biomed. Anal.*, 1998, **17**, 925.
[21] H. Poppe, Mass transfer in rectangular chromatographic channels, *J. Chromatogr. A*, 2002, **948**, 3.
[22] J. De Smet, P. Gzil, G.V. Baron and G. Desmet, On the 3-dimensional effects in etched chips for high performance liquid chromatography-separations, *J. Chromatogr. A*, 2007, **1154**, 189.
[23] K. Broeckhoven and G. Desmet, Numerical and analytical solutions for the column length-dependent band broadening originating from axisymmetrical trans-column velocity gradients, *J. Chromatogr. A*, 2009, **1216**, 1325.
[24] K. Vanderlinden, K. Broeckhoven, Y. Vanderheyden and G. Desmet, Effect of pre-and post-column band broadening on the performance of high-speed chromatography columns under isocratic and gradient conditions, *J. Chromatogr. A*, 2016, **1442**, 73.

Figure Captions

Figure 1. Geometries of the 4 different considered distributor types, **(a)** bifurcating (BF) **(b)** radially interconnected (RI) **(c)** mixed mode$_I$ (MM$_I$) **(d)** mixed mode$_{II}$ (MM$_{II}$). The red lines in (a)-(d) show the location of the species monitor line. The red boxes show the location of the tunable porous zone (2.5 µm x 2.5 µm) used to mimic clogging effects. **(e)** zoomed view of the inlet of the distributors and the grid size and shape. The dashed red box contains the 100 grid cells forming the species injection box. Channel width = 2.5 µm for every distributor, the flat-rectangular elements in the final row of each distributor are 30 µm wide and 2.5 µm thick.

Figure 2. Spatial species distribution just prior to the moment of elution in the absence of clogging at a flow rate of 1.32 µL/min for the **(a)** bifurcating (BF) **(b)** radially interconnected (RI) **(c)** mixed mode$_I$ (MM$_I$) **(d)** mixed mode$_{II}$ (MM$_{II}$) distributors. Only one half of each distributor is shown because of the symmetry line running through the center of each distributor. Color scales linear with concentration (red=maximum, blue=0).

Figure 3. Time responses of the species bands recorded at the monitor line in the absence of clogging for the cases shown in Fig. 2. The response is defined as the line integral of the mass fraction of species over the monitor line.

Figure 4. Effect of 70 % clogging in the indicated red box on the species band just prior to the moment of elution at a flow rate of 1.32 µL/min for the **(a)** bifurcating (BF) **(b)** radially interconnected (RI) **(c)** mixed mode$_I$ (MM$_I$) **(d)** mixed mode$_{II}$ (MM$_{II}$) distributors. Only one half of each distributor is shown because of the symmetry line running through the center of each distributor. The dashed ovals denote the species that entered the clogged channel, the red curved arrow indicates the leakage of species from the unclogged area to the clogged area in the BF-distributor. Color scales linear with concentration (red=maximum, blue=0).

Figure 5. Time responses of the species bands recorded at the monitor line for the cases shown in Fig. 4 (70 % clogging). The response is defined as the line integral of the mass fraction of species over the monitor line. The arrow shows the extra peak appearing for the MM$_I$-distributor caused by the species that entered the clogged channel and hence leave the distributor later.

Figure 6. Volumetric variance σ_v^2 of the species band recorded at the monitor line as a function of the applied flow rate for the RI- (squares), MM$_I$- (triangles) and BF- (diamonds) distributors (width = 500 µm, 16 outlets) in the absence of clogging.

Figure 7. Volumetric variance σ_v^2 (data points) of the species band recorded at the monitor line as a function of the final distributor width (or number of outlets) in the absence of clogging (squares: RI, triangles: MM$_I$, and diamonds: BF,) together with a power law fit (lines). The applied flow rate was

adjusted for each distributor width to keep the same linear velocity (0.25 mm/s) in the subsequent bed.

Figure 8. Volumetric variance σ_v^2 of the species bands recorded at the monitor line as a function of the degree of clogging in the red boxes indicated in Fig. 1 for the 500 µm wide (16 outlets) RI- (squares),MM_I- (triangles) and BF-distributors (diamonds). Flow rate = 1.32 µL/min (corresponding to a linear velocity of 0.25 mm/s in the subsequent bed).

Figure 1

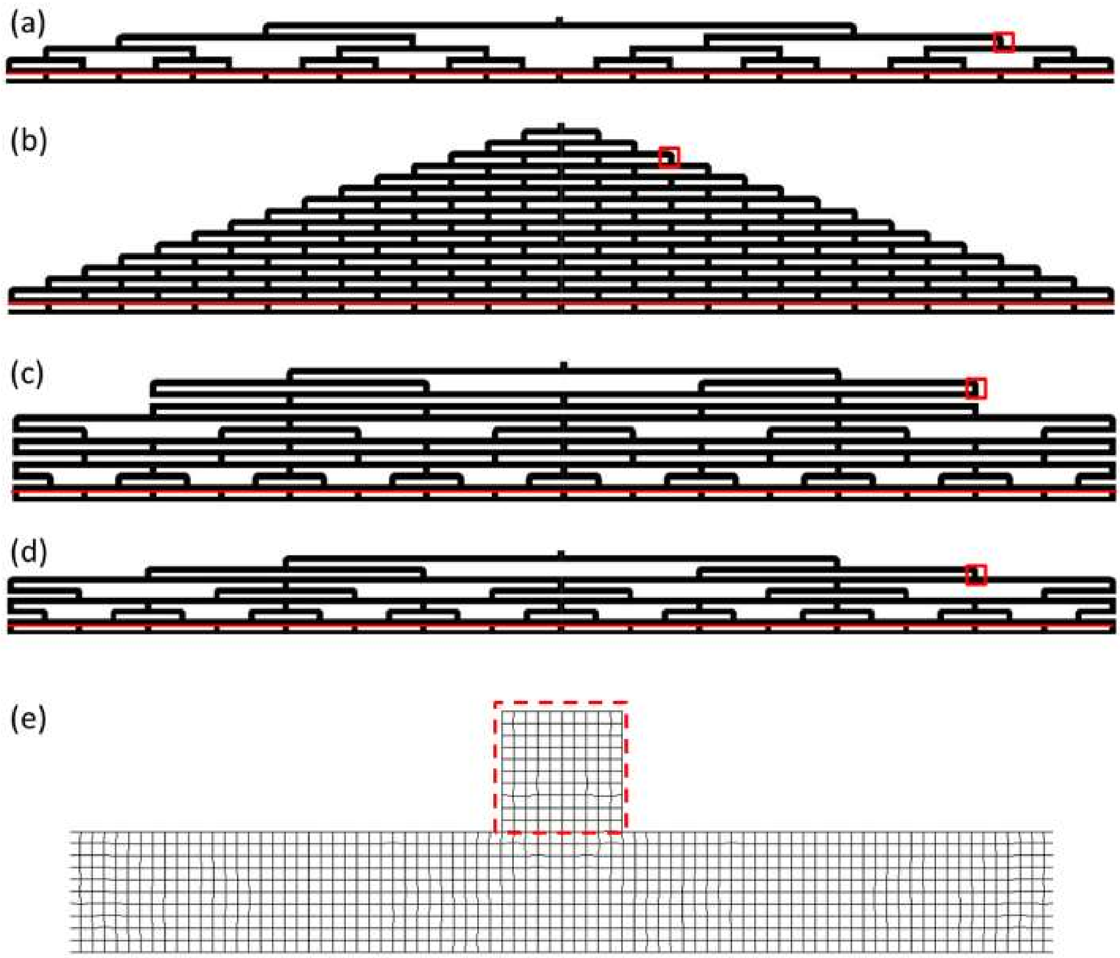

Figure 2

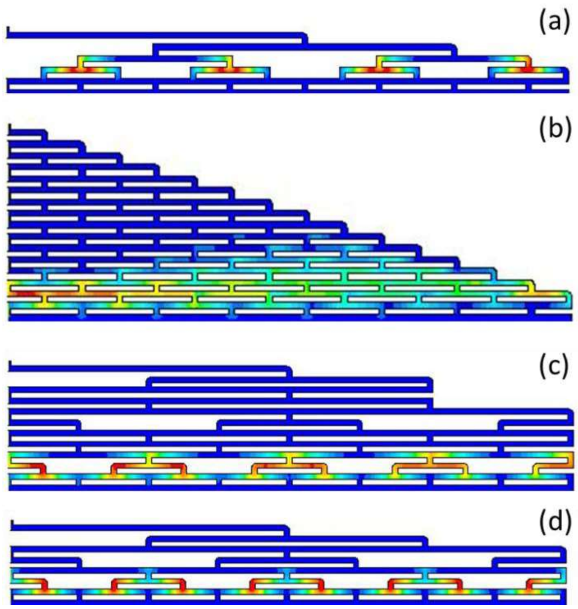

Figure 3

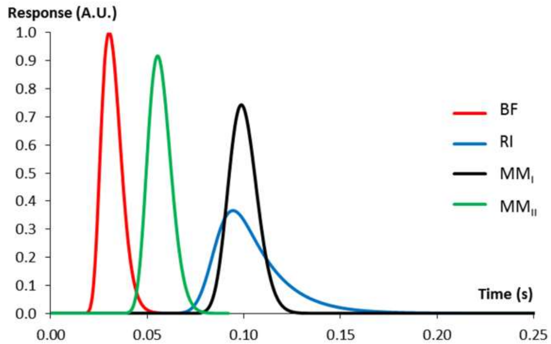

Response (A.U.)
1.0
0.9
0.8
0.7
0.6
0.5
0.4
0.3
0.2
0.1
0.0
BF
RI
MM$_I$
MM$_{II}$
Time (s)
0.00
0.05
0.10
0.15
0.20
0.25

Figure 4

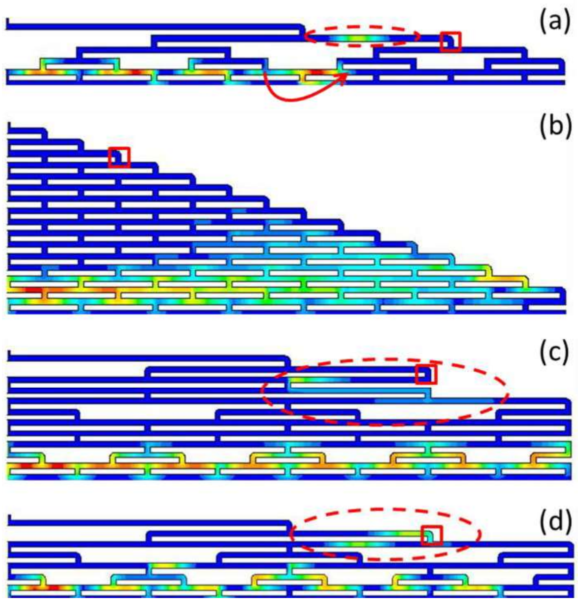

Figure 5

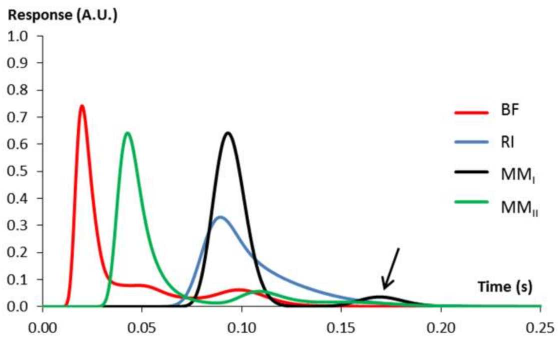
Response (A.U.)
1.0
0.9
0.8
0.7
0.6
0.5
0.4
0.3
0.2
0.1
0.0
0.00
0.05
0.10
0.15
0.20
0.25
Time (s)
BF
RI
MM_I
MM_{II}

Figure 6

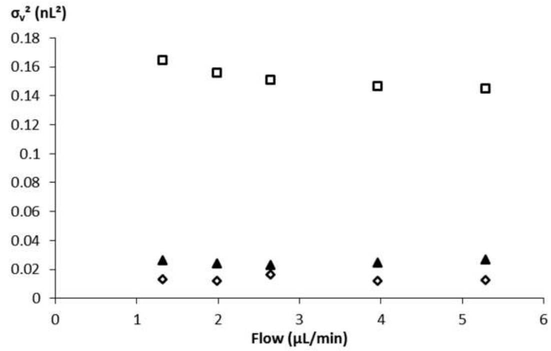

Figure 7

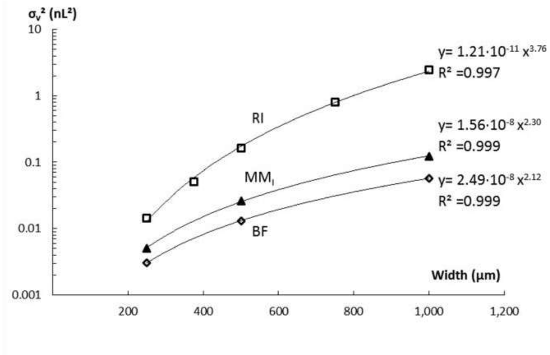

σv² (nL²)
10
1
0.1
0.01
0.001
200
400
600
800
1,000
1,200
Width (µm)
RI
MMI
BF
y= 1.21·10-11 x3.76
R² =0.997
y= 1.56·10-8 x2.30
R² =0.999
y= 2.49·10-8 x2.12
R² =0.999

Figure 8

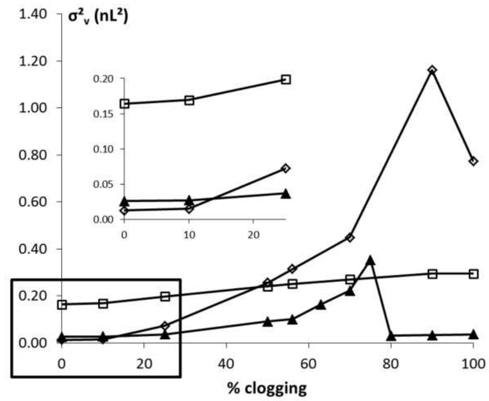

σ²v (nL²)
1.40
1.20
1.00
0.80
0.60
0.40
0.20
0.00
0
20
40
60
80
100
% clogging
0.20
0.15
0.10
0.05
0.00
0
10
20

Tables

Table 1. Comparison of mean elution, volumetric variance, and pressure drop for the different distributor types in the absence of clogging at a flow rate of 1.32 μL/min.

	RI	**MM_I**	**MM_{II}**	**BF**
$\bar{t}$ (s)	0.100	0.100	0.057	0.032
σ_v^2 (nL^2)	0.165	0.026	0.017	0.013
Δp (bar)	3.5	11.2	8.7	7.7

Table 2. Comparison of the mean elution time and the volumetric variance for the different distributor types with 70 % clogging of the outer most channel at the 4-outlet-level and a flow rate of 1.32 μL/min.

	RI	**MM_I**	**MM_{II}**	**BF**
$\bar{t}$ (s)	0.100	0.100	0.061	0.040
σ_v^2 (nL^2)	0.271	0.223	0.532	0.450